Journal of Hazardous Materials 192 (2011) 691–697

Contents lists available at ScienceDirect

Journal of Hazardous Materials

journal homepage: www.elsevier.com/locate/jhazmat

Application of fly ash as a catalyst for synthesis of carbon nanotube ribbons

Dilip C.D. Nath*, Veena Sahajwalla

Centre for Sustainable Materials Research and Technology, School of Materials Science and Engineering, The University of New South Wales, Sydney, NSW 2052, Australia

ARTICLE INFO

Article history:
Received 12 December 2010
Received in revised form 29 April 2011
Accepted 22 May 2011
Available online 27 May 2011

Keywords:
Fly ash
Carbon nanotube
Poly (vinyl alocohol)
Composite film and interface

ABSTRACT

The larger diameter-based carbon nanotube (CNT) ropes and ribbons are currently synthesized by catalytic decomposition of hydrocarbons with transition metal-based catalysts e.g., Co, Ni, Fe and Mo at 1100–1200 °C, using chemical vapour deposition (CVD) and electric arc methods. We produced CNT ribbons by fly ash (FA) catalyzed pyrolysis of a composite film of poly (vinyl alcohol) (PVA) with FA at 500 °C for 10 min under a nitrogen flow of 2 L/min. Different geometrical structures, e.g.; knotted and twisted, U- and spiral-shaped CNT ribbons were observed in the images of scanning and transmission electron microscopy. The widths of the CNT ribbons measured varied in the ranges 18–80 nm. X-ray photoelectron spectroscopy analysis showed five types of carbon binding peaks, C–C/C–H (~77%), C–O–H (~9%), –C–O–C (~5%), C═O (~5%) and –O–C═O (~3%). The ratio of intensities of G and D bands, *IG*/*ID* was 1.61 analysed by Raman Spectroscopy. CNT ribbons grown on the surface of FA have potential for the fabrication of high-strength composite materials with polymer and metal.

1. Introduction

CNT is a potential advanced material for wide ranges of applications, e.g. composites, devices for energy storage and energy conversion, electrodes, catalyst supports and sensors [1]. The self-assembly of CNT fiber/ribbon is a big challenging task using one-step fabrication process. CNT tying knots and ribbons with high flexibility were assembled by post-processing method using the aqueous solution of sodium dodecyl sulphate (SDS) and PVA [2], or blended with PVA solution/gels [3]. The threads of CNTs have been assembled as a result of van der Waal interactions on silicon substrate. Another post-processing method for the fabrication of CNT films was reported using the dispersed gel/solution of CNT in oleum followed by drying [4].

The CVD of hexane and thiophene in the presence of ferrocene catalyst in a furnace has generated the isolated fiber strands [5]. The pyrolysis of benzene at 1000 °C over Ni powder for 60 min also generated different types of carbon nanostructures materials [6]. Carbon nanocapsules with SiC nanoparticles were reported by thermal decomposition of PVA with SiC clusters at 500 °C in argon [7]. Catalytic graphitization of amorphous carbon formed in the pyrolysis of PVA with Fe-containing catalyst has happened in the frame of CNT structure at 600–800 °C in nitrogen flow for 2 h. The catalyst particles uniformly distributed on the surface and filled the hollow channel of CNT [8].

Coal combustion in power station generates a huge amount of FA as a by-product. The managements of FA consequently made a global concern on the environmental and economic points of view [9]. FA is generally disposed as landfill in the fulfilment of dams and lagoons. It is typically consisted of crystalline aluminosilicate, mullite and α-quartz along with trace amount of calcium, magnesium, potassium, sodium and titanium oxides, depending on the nature of coal burned. The particle size distribution patterns of the spherical-shaped FA are in the range of 1–100 μm based on the processing condition [10].

In 2007, the beneficial application of FA is counted less than 20% on the amount of total production ~14.5 million tons produced in Australia [11]. Research on recycling and reuse of FA as filler and catalyst/support has established an eco-friendly technology for value-added products and engineering composites. The successful beneficial applications of FA are agriculture and soil management, absorbents for heavy metals, waste stabilization, composite with polymer [10,12], cement and concrete [13], composite with metal [14] and catalyst/support [9,11].

Iron nitrate impregnated FA was recently used for the synthesis of multi-walled carbon nanotube (MWCNT) by CVD of the mixtures of gaseous precursors, ethylene, hydrogen and nitrogen at 700 °C for 30 min [11]. This method consumed costly ethylene and highly flammable hydrogen gas as well as an additional impregnation step for FA. There is no published report to present where FA is used alone as catalyst for the synthesis of self-assembled CNT ribbon structures even with non-metal catalyst. We present a pyrolysis method using composite of PVA and FA in which FA acts as a catalyst for the growth of self-assembled CNT ribbons along with different geometrical CNT structures.

* Corresponding author. Tel.: +61 2 9385 5130; fax: +61 2 9385 4292.
E-mail address: dilip.nath@unsw.edu.au (D.C.D. Nath).

0304-3894/$ – see front matter.
doi:10.1016/j.jhazmat.2011.05.072

Table 1
Mechanical properties of PVA and composite films.

FA (%)	Tensile strength (MPa)	Increased Strain (%)	Tensile strength (%)	Decreased strain (%)	Modulus (MPa)	Increased modulus (%)
0	28.2 ± 0.9	–	238 ± 10	–	120	–
25	88.4 ± 2	213.4	42 ± 2	82.3	334	178.3

2. Experimental

2.1. Materials and preparation of composite films

An industrial waste FA material was obtained from Swanbank Coal Fire Plant, Qld, Australia and used as received. PVA (Molecular weight, 125,000 g/mol; degree of hydrolysis ~89% with remaining acetate) from S.D. Fine-Chemical Ltd., Chennai, India was purchased and used as received. PVA composite film was fabricated by a casting method from an aqueous suspension of PVA and FA. PVA was dissolved in deionized water (Milli Q) at 80 °C to prepare the 1.2 wt% solution. FA particles (25 wt%) were dispersed and sonicated for 5 min. The resulting mixture was cast in glass petri dishes (10 cm diameter) and bubbles were removed by shaking and air blowing. The petri dishes were kept at room temperature until completely dry. The films were peeled out and dried in an oven at 60 °C under vacuum for 6 h. The thickness of the films was 50–70 μm [11].

2.2. Pyrolysis method

The pyrolysis of the samples was run at an isothermal condition in a horizontal quartz tube furnace (HQTF6035) under nitrogen flow. The hot zone of the furnace was preheated to 500 °C controlled using thermo couple. A diagram of the furnace setting was reported in our work [15]. The weighed amount of sample was kept in an alumina crucible and placed on a graphite feeder. Then it is inserted into the cold zone with simultaneous nitrogen purging at 2 L/min and held for 30 s, then passed through into the hot zone for 10 min. After pyrolysis, the sample was relocated from the hot to the cold zone via the graphite feeder for 30 s, and removed from the alumina crucible at room temperature. The sample was stored in a small sample bottle, and used for calculation and analysis.

2.3. Analysis and analytical instruments

The mechanical properties of the composite films were determined from tensile tests using an Instron 1185 with crosshead movement 50 mm/min. The specimens were prepared as per ASTM D882-95a (length 22 mm, width 5 mm) cut by a sharp razor blade. Four samples were tested in each category and averaged the results. The modulus values were calculated from the linear regions of stress–strain curves without an extensometer [10].

A Hitachi 4500-II scanning electron microscope (SEM) was used to examine the morphology of the sample. The sample on carbon tape was coated with chromium in a chromium sputter unit to improve conductivity. Transmission electron microscopy (TEM) images were obtained using a Philips CM200. The sample was dispersed in ethanol and a drop of diluted suspension was poured onto a carbon-coated copper grid, which was directly injected into a sample injection holder after air-drying for three days or longer.

X-ray photoelectron spectroscopy (XPS) was conducted using an ESCALAB220i-XL (VG Scientific, Thermo Scientific, UK) for the calculation of atomic compositions of samples. The standard conditions were used: $>2 \times 10^{-9}$ mbar, mono-chromate Al K alpha (energy 1486.6 eV), 200 W (20 mA and 10 kV), spot size ~1 mm in cross, photoelectron take-off angle of 90°, pass energy of 100 eV for survey scans and 20 eV for region scans, and step-size of 1 eV for survey scans and 0.1 eV for region scans. Raman spectroscopy was performed on an inVia Reinshaw Raman microscope using green laser excitation (514 nm). Scan was recorded on an extended range (100–4000 cm^{-1}) with 10% power of 1.2 mW. Sample was prepared by pressing onto a glass slide.

3. Results and discussion

3.1. Properties of PVA and composite films

The detailed physical, chemical and mineralogical analysis of FA and the high-strength biodegradable composite films of PVA with various concentration of FA were reported in our work [10]. The chemical analysis of FA mainly shows by oxide basis of elements, Si_2O 73.60%, Al_2O_3 18.70%, Fe_2O_3 1.90% and TiO_2 1.36% including with trace amount of CaO, BaO, MgO, MnO and P_2O_5. Silica and alumina are composed of with tetra and octahedral aluminosilicate structures of crystalline mineral phase, mullite [10].

A representative stress–strain relationship diagram of PVA and composite film with 25 wt% FA are presented in Fig. 1 and the data are displayed in Table 1. FA addition to PVA dramatically enhances the tensile strength by ~213% and decreases the strain at break by ~82%. PVA is a highly polar polymer matrix containing –OH groups and/or acetate group depending on the degree of hydrolysation that occurs during synthesis [16]. PVA used in this study is 89% hydrolysed containing two functional groups, hydroxyl and acetate.

The general phenomenon is that the hydroxyl groups cover the surfaces of metal and metalloid oxides [17]. This plays a significant role in the formation of physical bonding between the substrates. For example, silica was identified as a fully hydroxyl-covered powder material. FA consisted of ~74% silica therefore it was apparently believed that its surface was covered by hydroxyl groups. The existence of hydroxyl group on the FA and PVA formed a bridge-like physical bond which contributed the enhancement of composite's mechanical strength by transferring the local stress [10,17].

The mobility of PVA chains is inversely related to the formation of interfacial interactions between PVA and FA which is

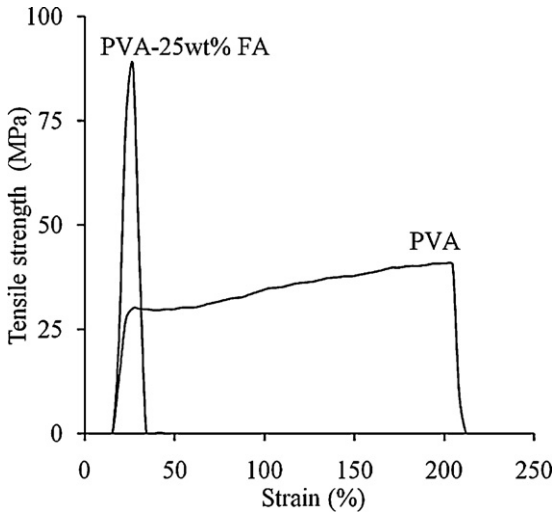

Fig. 1. The relationship of tensile strength and strain of films.

measured by glass transition temperature (T_g). T_g values for PVA is ~73 °C, and it goes up to ~10 °C higher for the composite material. This indicates that the restriction of segmental motion of PVA requires an additional energy to shift the amorphous domains in PVA due to the formation of web-like network between PVA and FA [10].

3.2. Pyrolysis of PVA and composite films

Powder PVA, the physical mixtures of powder PVA and FA, PVA and composite films were pyrolized. The yields of solid residues are shown in Table 2. Although the gaseous extract is not analysed, there are several studies on the analysis of gaseous extract formed by the pyrolysis of PVA under nitrogen [18]. These products are formed by depolymerization, dehydration and intra-molecular cyclization reactions of polyene sequences account for the formation of aromatic products in absence of catalyst. Hydrocarbons mainly consist of C6 compounds (gasoline, diesel oil and aromatics) and the gaseous composition is of 40.4 wt%, and H_2O 20.9 wt%, CO_2 19.2 wt% and CO 18.9 wt% based on total mass of gaseous products [18].

Table 2
Pyrolysis of PVA and FA composite film.[a]

PVA (g)	FA (g)	Composite film (g)	Solid residue (g)	Yield (%)
–	–	0.11 (25 wt% FA)	0.05	45.5
0.10	–	–	0.00	0
0.10	0.03	–	Trace (FA)	n.d.
–	0.20	–	0.18	90

[a] All experiments were done at 500 °C for 10 min.

The pyrolysis of PVA composite film with 25 wt% FA remained black solid residue on the alumina crucible. The calculated yield is 45.5% on the basis of film weight and solid residue. The pyrolysis of powder PVA did not produce any solid reside. In the pyrolysis of the physical mixtures of PVA and 25 wt% FA, the solid residue remain on the crucible belongs to only FA. The macroscopic contact area of PVA and FA by physical mixing did not show an active site for the initiation and propagation reaction in the growth of carbonaceous materials. The microscopic intimate

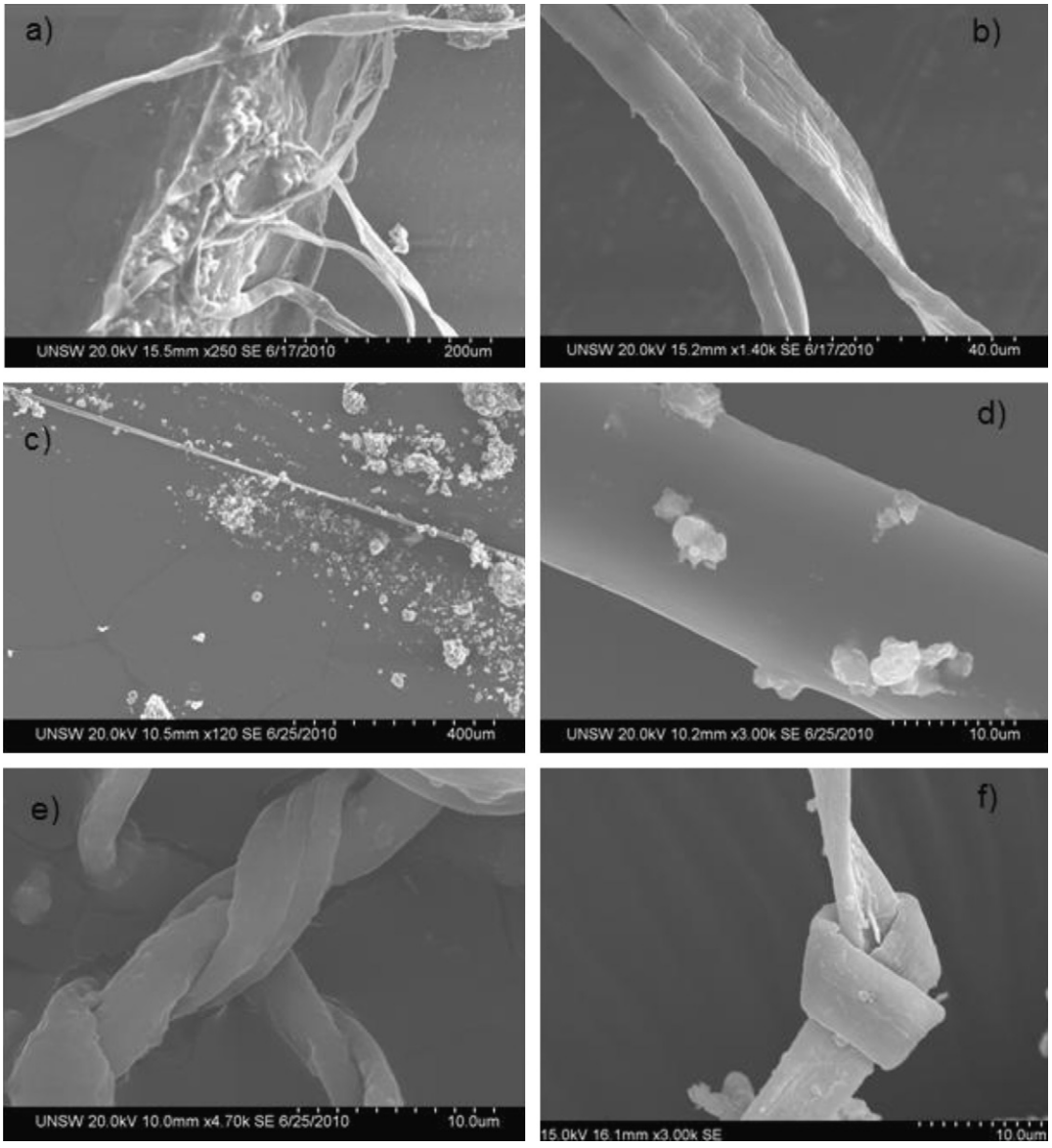

Fig. 2. SEM images of different morphological geometries, (a) CNT grown on active sites, (b) CNT ribbons, (c) single straight CNT, (d) higher magnification of image (c), (e) twisting behaviour of CNT ribbons and (f) a permanently knotted CNT ribbon structure.

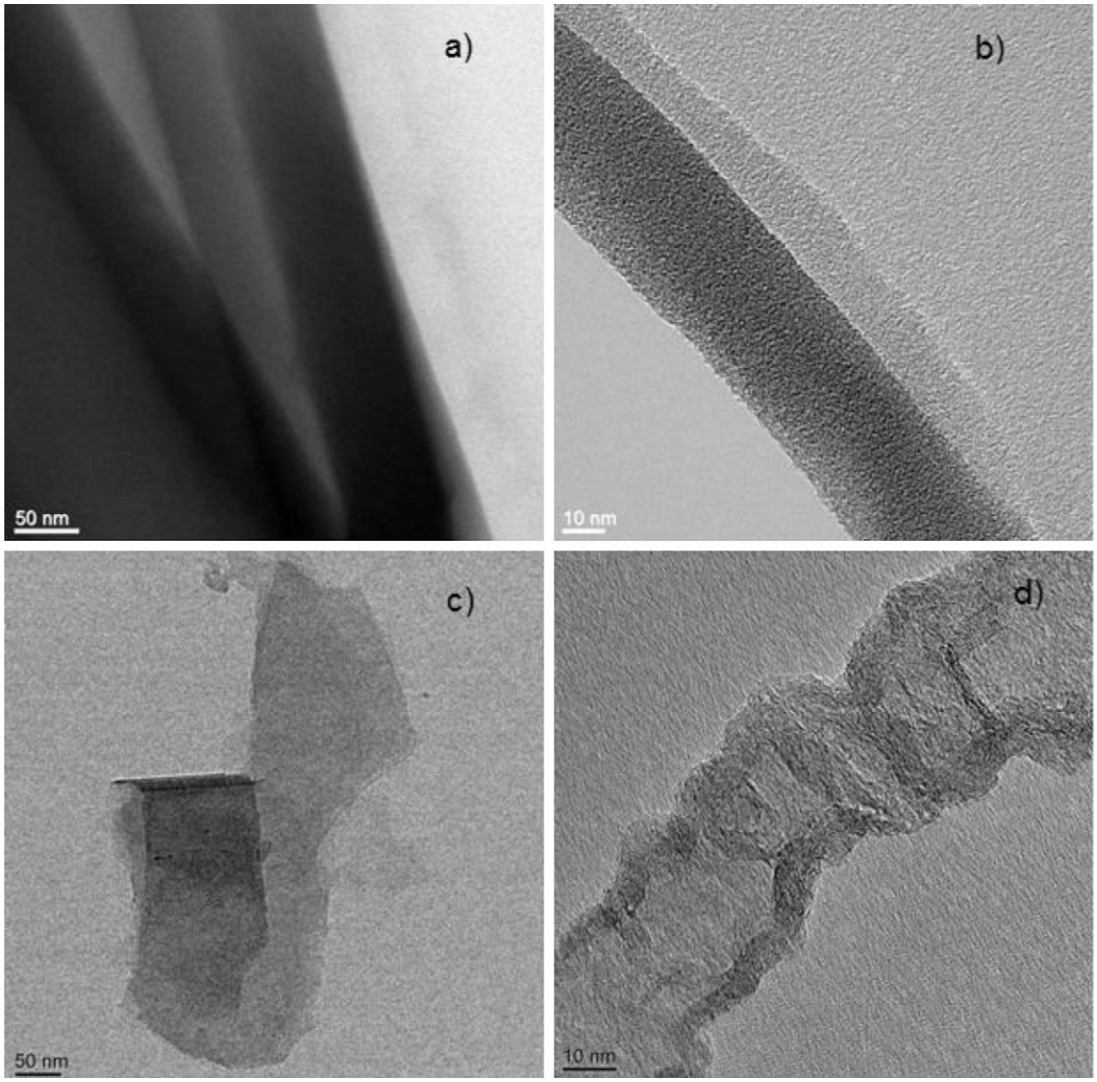

Fig. 3. TEM images of CNT, (a) growth of aligned CNT ribbons, (b) single ribbon, showing constant width, (c) U-shaped and (d) spiral-shaped CNT ribbon structures.

contact areas were visualized in SEM images of fractured-surface film in tensile test [10]. The interfacial interaction is prerequisite for the enhancement of mechanical strength and formation of catalytic active sites for growth of carbonaceous solid material.

3.3. Morphology of carbonaceous solid material

The morphology of the carbonaceous residue was analysed by SEM and TEM. The representative SEM images of different morphological geometries are displayed in Fig. 2(a–f). Fig. 2a clearly shows the active sites of CNT ribbons initiated and grown randomly on the FA surfaces. Fig. 2b reveals the selected area of bundle of long and flexible CNT ribbons which was captured with 40 μm scale bar.

The selected area of a straight CNT ribbon is shown with 400 and 10 μm scale bar in Fig. 2(c and d). The surface of CNT ribbons is not absolutely free from the FA particles. The selective adherences of FA particles on the surface CNT ribbon indicate the defect in graphitization where space/void remained for particle depositions and/or functionalized carbon which has strong interaction with FA. The functionalized carbon on CNT structures was found in XPS analysis which is discussed later.

Fig. 2(e–f) shows the microscopic permanently twisted and knotted of CNT ribbons. Several self-assembled fibers and ribbons of oriented CNT were reported by an additional and/or post processing methods [2,19–21]. For example, the self-assembled CNT fibers and ribbons were directly achieved by CVD at 1200 °C using liquid source of carbon on the support of iron catalyst under hydrogen flow [19]. A series of liquid carbon sources were used e.g., ethanol with diethylether, polyethylene glycol, 1-propanol, acetone and ethylformate using iron catalyst in the combination of ~2.3 wt% ferrocene and ~4.0 wt% thiophene.

The well-aligned and permanent-twisted CNT fibers were visualized under SEM observation. The details of the fabrication procedure using cobalt catalyst and various morphologies of thin coiled well-graphitized nanotubules were produced with acetylene as carbon source [20]. The morphologies of CNT obtained showed single and straight, pair of parallel tubules binding together by van der Waals attraction and complicated interactions between straight and helix-shaped tubules along with planar spiral-shaped tubule.

Although the twisted assembly of CNT has also been found in an expensive/complicated system [21], the self-assembly of CNT alone by the pyrolysis of composite with FA has not yet been reported. The knitting and knotting of CNT were reported with PVA as composite yarns of various geometries. For example [21], the aligned CNT forests were synthesized in CVD using 5 mol% C_2H_2 under helium at 680 °C on an iron-catalyst film deposited on a silicon wafer substrate.

Table 3
Elemental peak list in CNT and FA determined by XPS.

CNT				FA			Detailed C 1s peak			
Core level	Peak (eV)	FWHM (eV)	atm (%)	Peak (eV)	FWHM (eV)	atm (%)	Core level	Peak (eV)	FWHM (eV)	atm (%)
Al 2p	74.7	3.4	1.8	74.1	1.6	5.5	C–C/C–H	285.1	1.2	76.6
Si 2p	103.7	3.2	6.7	102.9	1.8	24.9	C–O–H	286.6	1.2	9.6
C 1s	285.2	3.2	56.7	284.8	2.1	4.1	C–O–C	288.1	1.3	4.7
Ca 2p	348.4	3.4	2.9	347.7	0.8	0.2	C=O	289.2	1.3	5.6
O 1s	532.2	3.5	29.3	532.6	1.8	59.2	O–C=O	290.3	1.3	3.2
Na1s	1072.1	3.1	1.7	1073.5	2.5	3.6				

The synthesized CNT was used to fabricate CNT yarns with aqueous solution of PVA. The yarns of CNT/PVA composite were made either by soaking a single yarn in 5 wt% aqueous PVA solution for 15 h or by passing a single yarn through this solution during spinning followed by drying. The designed yarns show various microscopic geometries like, single, two-ply, four-ply, knitted and knotted CNT yarns [21].

We use an eco-friendly safe method using waste feedstock for the assembly of CNT into indefinitely long ribbons and fibers with different geometries. CNT ribbons show highly flexible and permanently twisted/knotted ribbon structures at microscopic scales. The interpretation for the formation of knot is that it happens when the multi-directional growing CNT end moves through a formed ribbon loop by van der Waals attraction. A post-processing method has been reported [2], consisting of the dispersal of CNT in a solution of surfactant, SDS and their recondensing against the flow of PVA solution to form a nanotube mesh. The mesh then transformed into fiber. The synthesized CNT fibers were able to be strongly bent and tightly tied knot without breaking.

Fig. 3(a–d) shows the representative TEM images of different morphological geometries of CNT ribbons. The growth of CNT ribbons with different widths observes in Fig. 3a. In the higher magnification of a single ribbon in Fig. 3b, it shows the ribbon structure clearly with ~19 nm constant width throughout the length. The widths of the ribbons measured vary in the ranges 18–80 nm. Fig. 3(c and d) reveals a U-shaped and a branched/spiral-shaped geometry of CNT ribbons. We also found some graphene sheets to be rolled in our SEM/TEM images. No significant effects of the concentration of FA, temperature and time on the structures of CNT were observed in the system.

Although several authors have widely studied on the growth of CNT by the decomposition of hydrocarbons on metal surfaces, Fe, Co, Cu and Ni at ~1200 °C, the exact mechanism is still hypothetical. Considering the growth mechanism mentioned elsewhere [22], we have recently proposed a diagram to show the overall growth mechanism on the results obtained in the pyrolysis of PVA composite with FA [15]. We proposed that at 500 °C, the partially attached hydrogen atoms and hydroxyl groups of PVA with FA surfaces were abstracted in the form of hydrogen and water molecules. The cleavage PVA chain transformed into carbon–carbon double-bonded sp^2 conformation as carbon fragments. The sizes of the carbon fragments depend on the degree of polymerization of PVA on the basis of a broken TEM image of CNT by sonication [15].

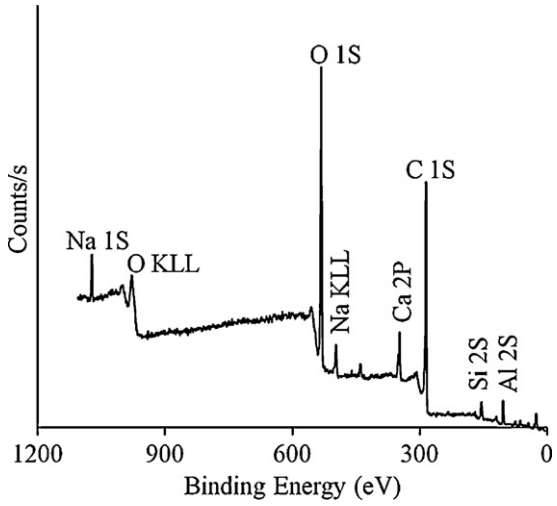

Fig. 4. Wide range XPS spectrum of CNT grown on FA surfaces.

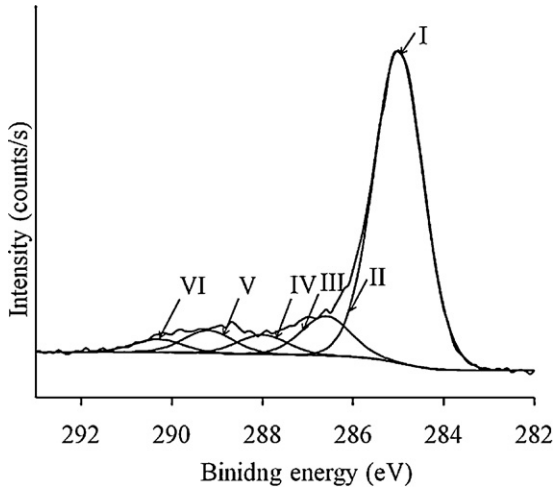

Fig. 5. Extended peak of C 1s from wide range CNT spectrum in Fig. 4, (I) raw peak, (II) C–C/C–H configuration, (III) C–O–H configuration, (IV) C–O–C configuration, (V) C=O configuration and (VI) –COOH/–$COOCH_3$ configuration.

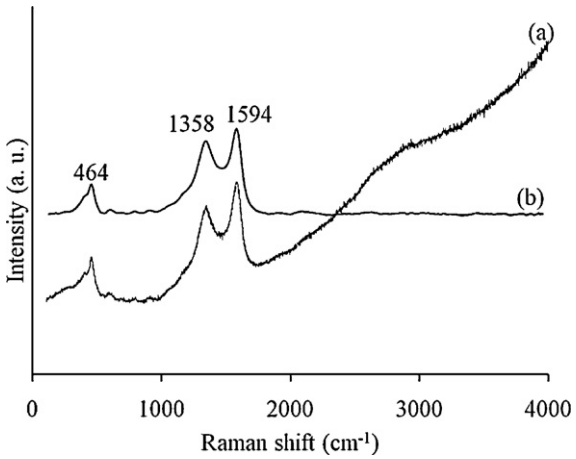

Fig. 6. Raman spectra of CNT, (a) raw spectrum and (b) baseline-corrected spectrum with multiple points.

3.4. XPS and Raman study for characterization of CNT materials

XPS analyses were performed to determine the atomic concentration along with functionality of carbon in the structure of CNT ribbons. Fig. 4 shows the XPS wide survey spectrum recorded on ESCALAB220i-XL. All peaks were assigned using XPS reference handbook [23]. The peaks at 284.6 eV and 535 eV from the C 1s and O 1s core levels, respectively were generated by photoelectrons emitted. Although oxygen is one of the major elements in FA sample, the intensity of O 1s core is much higher compared with Si and Al 2s cores.

The details of calculated results, peak position with full width half maximum (FWHM) and atomic compositions (atm%) in CNT and FA are summarized in Table 3. The relative concentration of oxygen and carbon are found to be ~30% and ~57%, respectively, the remainders are mixtures of Na, Si, Ca and Al in CNT, whereas the percentage of O, Si and Al were found to be ~60%, ~25% and ~6%, respectively in FA. The extended region of the C 1s peak shows a broader area in the region of higher binding energy. The C 1s core peak therefore is separated into five different types of peaks by Lorentzian curve fitting method, showing the carbon oxidized groups in Fig. 5 and the calculated results of C 1s peak are displayed in Table 3.

The peak at 285.1 eV is generated by excitation of C–C/C–H (~77%) bonds in the graphite configuration including their shake-up structure, and peak centred at 286.6 eV is attributed to photoelectrons emitted from carbon bonding of C–O–H configuration with 9.6%. There are three other small peaks centred at 288.1, 289.2 and 290.3 eV emitted from carbon belonging to C–O–C (4.7%), –C=O (5.6%) and –COOH/–$COOCH_3$ (3.2%) groups, respectively. The oxygen containing functional groups grafted at CNT ribbons will be the precursors of the acetate nucleation sites in PVA backbones. Acid treatment functionalized the carbons on the CNT structure with different types of functional groups, e.g., C–O–H, C–O–C, C=O and –COOH/–$COOCH_3$ and analysed with XPS/IR spectra [3,22].

The graphitic configurations of CNT ribbons were also analysed by Raman spectroscopy. Raman spectroscopy is considered one of the most analytical tools for the characterization of carbon structures in CNT architectures. The raw spectrum along with baseline-corrected one by selection of multiple points is shown in Fig. 6 after excitation with 514 nm laser light. The characteristic bimodal peaks at 1358 and 1594 cm^{-1} were analysed. The strongest Raman G-line which is characteristic peak for well-graphitized CNT is appeared at 1594 cm^{-1} with 87 cm^{-1} FWHM.

The other peak at 1358 cm^{-1} along with 109 cm^{-1} FWHM is D-line, indicating a typical sign for defective graphitic structures on CNT. The intensity of D-line is lower than that of the G-line, indicating the more ordered carbon structure in CNT ribbons. CNT ribbons are consisted mainly of amorphous and crystalline graphitic carbons.

The intensity ratios (*I*G/*I*D) of the G peak (graphitic carbon) and D peak (defective carbon) is treated the degree of graphitization of carbon in CNT configuration [11]. The higher *I*G/*I*D ratio is the direct indication of the greater degree of well wall graphitization. The *I*G/*I*D ratio of our CNT ribbons was found to be 1.61 which was higher than the values 1.17 yielded by iron nitrate coated FA catalyst by CVD method using gaseous sources, the mixtures of ethylene, hydrogen and nitrogen [11]. The line width and intensity ratio of (*I*G/*I*D) vary depending on the structure of the carbons and the conditions used for analysis, e.g.; laser power and energy [24]. For example, Raman intensities and band-widths increased with the wave number of exciting laser from 742 to 457 nm, whereas the lines were shifted to lower wave numbers with the increasing wavelength of the exciting lasers [25].

Another behaviour is that the intensity ratios of *I*G/*I*D decrease non-linearly with the increasing of laser energy depending on the different types of tubes and graphite crystallites [22]. The broadening of the bands relates to the disorder within the carbon sheet and curve-natured CNT due to the enhancement of the electron–phonon coupling. The increases of electron–phonon coupling generally result from the admixture of σ to π bonded carbon atoms [24]. The overlapping peaks of silica of FA and radial breathing mean (RBM) of CNT ribbons were observed in the regions lower than <500 cm^{-1}.

4. Conclusions

We presented the synthesis method of CNT materials by the pyrolysis of composite film of PVA and FA. The key points are: (i) CNT ribbon structures can be synthesized from sustainable waste polymer composite of PVA-FA by pyrolysis at low temperature, 500 °C for 10 min, (ii) Interfacial bonding between PVA and FA is a critical factor in achieving CNT structural materials, (iii) CNT ribbons are self-assembled with different geometric forms, e.g. fiber, knotted/twisted ribbons, graphene sheet and spiral with complicated configurations, (iv) the widths of self-assembled CNT ribbons measured are in the ranges of 18–80 nm, (v) eco-friendly CNT material with FA is a potential filler material for the fabrication of composites with metal and polymer. The process is a promising recycling paradigm for the management of sustainable waste materials by achieving value-added advanced products.

References

[1] S. Huang, X. Cai, J. Liu, Growth of millimeter-long and horizontally aligned single-walled carbon nanotubes on flat substrates, J. Am. Chem. Soc. 125 (2003) 5636–5637.
[2] B. Vigolo, A. Penicaud, C. Coulon, C. Sauder, R. Pailler, C. Journet, P. Bernier, P. Poulin, Macroscopic fibers and ribbons of orientated carbon nanotubes, Science 290 (2000) 1331–1334.
[3] A.B. Dalton, S. Collins, E. Munoz, J.M. Razal, V.H. Ebron, J.P. Perraris, J.N. Coleman, B.G. Kim, Super-tough carbon-nanotube fibres, Nature 423 (2003) 703–1703.
[4] T.V. Sreekumar, T. Liu, S. Kumar, L.M. Ericson, R.H. Hauge, R.E. Smalley, Single-wall carbon nanotube films, Chem. Mater. 15 (2003) 175–178.
[5] B. Wei, R. Vajtai, Y.Y. Choi, P.M. Ajayan, Structural characterizations of long single-walled carbon nanotube strands, Nano Letters 2 (10) (2002) 1105–1107.
[6] M. Benito, Y. Maniette, Y. Aniette, E. Mogoza, T.M. Martnez, Carbon nanotubes production by catalytic pyrolysis of benzene, Carbon 36 (5–6) (1998) 681–683.
[7] T. Oku, K. Niihara, K. Suganuma, Formation of carbon nanocapsules with SiC nanoparticles prepared by polymer pyrolysis, J. Mater. Chem. 8 (6) (1998) 1323–1325.
[8] O.P. Krivoruchko, N.I. Maksimova, V.I. Zaikovskii, A.N. Salanov, Study of multi-walled graphite nanotubes and filaments formation from carbonized products of polyvinyl alcohol via catalytic graphitization at 600–800 °C in nitrogen atmosphere, Carbon 38 (2000) 1075–1082.
[9] S. Wang, Application of solid ash based catalysts in heterogeneous catalysis, Environ. Sci. Technol. 42 (19) (2008) 7055–7063.
[10] D.C.D. Nath, S. Bandyopadhyay, P. Boughton, A. Yu, D. Blackburn, C. White, High strength biodegradable poly(vinyl alcohol)/fly ash composite films, J. Appl. Polym. Sci. 117 (2010) 114–121.
[11] O.M. Dunens, K.J. Mackenzie, A.T. Harris, Synthesis of Multiwalled carbon nanotubes on fly ash derived catalysts, Environ. Sci. Technol. 43 (2009) 7889–7894.
[12] D.C.D. Nath, S. Bandyopadhyay, A. Yu, Q. Zeng, T. Das, D. Blackburn, C. White, Structure–property-interface correlation of fly ash–*isotactic* polypropylene composites, J. Mater. Sci. 44 (2009) 6078–6089.
[13] J.P. Gorninski, D.C.D. Molin, C.S. Kazmierczak, Study of the modulus of elasticity of polymer concrete compounds and comparative assessment of polymer concrete and portland cement concrete, Cem. Concr. Res. 34 (2004) 2091–2095.
[14] P.K. Rohatgi, N. Gupta, S. Alaraj, Thermal expansion of aluminum–fly ash cenosphere composites synthesized by pressure infiltration technique, J. Compos. Mater. 40 (13) (2006) 1163–1173.
[15] D. Nath, V. Sahajwalla, Growth mechanism of carbon nanotube produced by pyrolysis of a composite film of poly (vinyl alcohol) and fly ash, Appl. Phys. A, doi:10.1007/s00339-011-6405-1, in press.
[16] E. Chiellini, P. Cinelli, S.H. Imam, I. Mao, Composite films based on biorelated agro-industrial waste and poly(vinyl alcohol). Preparation and mechanical properties characterization, Biomacromolecules 2 (2001) 1029–1037.
[17] R. Mueller, H.K. Kammler, K. Wegner, S.E. Pratsinis, OH surface density of SiO_2 and TiO_2 by thermogravimetric analysis, Langmuir 19 (2003) 160–165.
[18] J.L. Shie, Y.H. Chen, C.Y. Chang, J.P. Lin, D.J. Lee, C.H. Wu, Thermal pyrolysis of poly (vinyl alcohol) and its major products, Energy Fuels 16 (2002) 109–118.
[19] Y.L. Li, I.A. Kinloch, A.H. Windle, Direct spinning of carbon nanotube fibers from chemical vapor deposition synthesis, Science 304 (2004) 276–278.

[20] S. Amelinckx, X.B. Zhang, D. Bernaerts, X.F. Zhangt, V. Ivanov, J.B. Nagy, A formation mechanism for catalytically grown helix-shaped graphite nanotubes, Science 265 (1994) 635–639.
[21] M. Zhang, K.R. Atkinson, R.H. Baughman, Multifunctional carbon nanotube yarns by downsizing an ancient Technology, Science 306 (2004) 1358–1361.
[22] A.A. Didik, V.I. Kodolov, A.Y. Volkov, E.G. Volkova, K.H. Hallmeier, Low-temperature growth of carbon nanotubes, Inorg. Mater. 39 (6) (2003) 583–587.
[23] J.F. Moulder, W.F. Stickle, P.E. Sobol, K.D. Bomben, Handbook of X-ray Photoelectron Spectroscopy, Perkin Elmer Corporation, USA, 1992, ISBN 0-9627026-2-5.
[24] J. Kastner, T. Pichler, H. Kuzmany, S. Curran, W. Blau, D.N. Weldon, M. Delamesiere, S. Draper, H. Zandbergen, Resonance Raman and infrared spectroscopy of carbon nanotubes, Chem. Phys. Lett. 221 (1994) 53–58.
[25] Y. Andoa, X. Zhaoa, H. Shimoyama, Structure analysis of purified multiwalled carbon nanotubes, Carbon 39 (2001) 569–574.